Check for updates

Pioneering Carboxylated Zirconium Oxo Cluster Resist for Precision Nanoscale Patterning

*Seong-Ji Ha, Jong-Chul Yoon, Minkyeong Kim, Bo Kyu Kwon, Doojin Jeon, Seung Gyu Gyeong, and Ji-Hyun Jang**

As the demand for nanoscale semiconductors grows, Advanced resist materials for next-generation lithography becomes increasingly critical. Expanding the range of available resists, particularly those incorporating metals, is essential to advancing lithographic technologies. Metal-based photoresists have attracted attention due to their inherently high etch resistance, yet many suffer from poor pattern robustness, limited solution stability, and the need for photoacid generators (PAGs). Here, a zirconium (Zr)-based oxo cluster bonded with benzoic acid (Zr-OCB) photoresist that overcomes these limitations through a molecular design strategy is presented. This molecularly designed resist strengthens patterned features through dimerization and oligomerization under exposure, while benzoate ligands provide stability via strong coordination with the Zr cluster. This study demonstrates a new class of structurally defined, PAG-free metal-based hybrid resists with superior pattern fidelity and formulation stability. This allowed for the formation of high-resolution patterns with a feature size of sub-40 nm, a sensitivity of 1905 µC cm^{-2}, a low line edge roughness of 3.1 nm, and excellent solution stability for up to 6 months, highlighting its potential for industrial applications. This work presents a promising Zr-based hybrid resist, offering enhanced stability and simplified processing, making it a valuable candidate for next-generation lithography.

1. Introduction

The evolution of electronic devices, such as cell phones and computers, has been deeply impacted by the vital role of semiconductors.[1–3] Progress in semiconductor technology has fueled the miniaturization of these devices, enhancing portability and satisfying the increasing demand for low power consumption and high performance.[4–9] With the rise of artificial intelligence, the need for faster and more energy-efficient semiconductors is growing, which in turn drives the development of advanced patterning technologies.[10–12] Traditional light sources, ranging from 436 nm g-Line to 193 nm ArF, have been instrumental in fine patterning.[13–18] However, the industry now seeks patterning technologies that can surpass the limitations of conventional optical lithography, particularly in achieving sub-10 nm resolution.[19] Among various next-generation approaches, electron beam lithography (EBL) is well-suited for fabricating high-resolution and customized nanoscale patterns, owing to its maskless and direct-write nature.

Despite these advantages, EBL photoresists face several limitations related to resist materials.[20] Polymer-based resists such as PMMA and SU-8 can achieve fine feature sizes, but typically require high exposure doses that lead to pattern collapse or bridging defects, and suffer from low etch resistance.[21–23] To overcome these limitations, metal-containing photoresists have been proposed, leveraging the high atomic number and radiation responsiveness of metals to improve sensitivity and etch durability.[24]

Among these, zirconium-based hybrid materials are particularly promising due to zirconium's ability to form strong, multidentate metal–ligand bonds, enabling the construction of well-defined metal oxo complexes.[25–28] These Zr-oxo clusters can undergo dimerization and oligomerization upon irradiation, providing enhanced mechanical integrity in patterned structures—an essential factor for negative-tone photoresists.[29,30] Notably, alkene-functionalized zirconium oxide systems have shown improved sensitivity and etch resistance through sol–gel synthesis routes.[31]

Nevertheless, many metal-based photoresists rely on poorly defined inorganic clusters, and significant challenges remain. Many metal-based photoresists rely on poorly defined inorganic clusters, leading to poor film homogeneity and limited solution stability. Additionally, the use of photoacid generators (PAGs) in these systems introduces complications such as acid diffusion,

S.-J. Ha, J.-C. Yoon, M. Kim, B. K. Kwon, D. Jeon, S. G. Gyeong, J.-H. Jang
School of Energy and Chemical Engineering
Graduate School of Semiconductor Materials and Device Engineering
Graduate School of Carbon Neutrality
UNIST
Ulsan 44919, Republic of Korea
E-mail: clau@unist.ac.kr

The ORCID identification number(s) for the author(s) of this article can be found under https://doi.org/10.1002/admt.202501547

© 2025 The Author(s). Advanced Materials Technologies published by Wiley-VCH GmbH. This is an open access article under the terms of the Creative Commons Attribution License, which permits use, distribution and reproduction in any medium, provided the original work is properly cited.

DOI: 10.1002/admt.202501547

2365709x, 0, Downloaded from https://advanced.onlinelibrary.wiley.com/doi/10.1002/admt.202501547 by Ulsan National Institute Of, Wiley Online Library on [13/10/2025]. See the Terms and Conditions (https://onlinelibrary.wiley.com/terms-and-conditions) on Wiley Online Library for rules of use; OA articles are governed by the applicable Creative Commons License

pattern blur, and standing wave effects, which compromise resolution and pattern fidelity.[32,33] In the case of Zr-based systems, issues like scumming, the retention of undeveloped resist, have also been reported, often attributed to ambient contamination or thermal interactions during post-exposure processing.[26,34]

In this study, we introduce a molecularly engineered zirconium oxo cluster photoresist (Zr-OCB) that addresses these key limitations. The design leverages three core innovations: 1) Zr oxo cluster that facilitates radiation-induced dimerization and oligomerization, reinforcing pattern robustness; 2) Benzoate ligands that afford solution stability through strong coordination; 3) PAG-free crosslinking mechanism based on carbon-centered radicals, enabling simplified formulation and high-resolution patterning without additive complications.

This approach provides a new molecular-level strategy for metal-based resist design, combining patterning precision, structural stability, and high etch resistance in a single platform. This paves the way for next-generation high-resolution nanopatterning, showing great potential to enhance the precision of integrated circuits in advanced lithography technologies.

2. Results and Discussion

We developed a Zr-based MOC photoresist, optimized with an ideal zirconium precursor/benzoic acid ratio, for next-generation lithography. The Zr-based resist was synthesized using a straightforward, one-step process involving a Zr oxo cluster and benzoic acid organic ligand, followed by a solvothermal process, as shown in **Figure 1a**. Our synthesis method offers several advantages, including rapid reaction, high material purity, and scalability for mass production.[35]

During the solvothermal reaction, benzoic acid undergoes dehydrogenation, forming benzoate, which binds to two Zr atoms in the Zr oxo cluster. As a result, we synthesized the Zr oxo cluster bonded with benzoic acid, referred to as Zr-OCB.

To confirm the coordination of Zr oxo clusters with benzoate groups in the material—a key indicator of successful Zr-OCB synthesis – we first investigated the interactions between the Zr oxo cluster and benzoic acid molecules in Zr-OCB resists using Fourier-transform infrared (FT-IR) spectroscopy. Figure 1b shows prominent peaks at 3690–3200 cm^{-1} (OH stretching), 3100–3000 cm^{-1} (aromatic CH stretching), 1700–1470 cm^{-1} (conjugated C═O and aromatic C─C stretching), 1460–1320 cm^{-1} (aromatic C═C stretching), 1190–1140 cm^{-1} (Zr–O–C stretching), and 730–670 cm^{-1} (Zr–O stretching), corresponding to asymmetric and symmetric stretching vibrations.[36–38] Further confirmation of Zr-OCB formation was obtained through ^{1}H NMR spectroscopy, as detailed in Figure S1 (Supporting Information). The signals ≈7–8 ppm are attributed to benzoate bonds with the Zr oxo cluster, while resonances at 1.03, 3.78, and 4.34 ppm suggest the presence of isopropyl alcohol weakly associated with the Zr oxo cluster. The X-ray diffraction (XRD) pattern of the synthesized Zr-OCB material exhibits broad features with no distinct diffraction peaks, indicating an amorphous structure. This observation supports the idea that the Zr oxo clusters do not form long-range ordered crystalline domains, consistent with the proposed coordination-based molecular architecture.[39]

Matrix-assisted laser desorption/ionization–time-of-flight mass spectrometry (MALDI-TOF MS) analysis of the Zr-OCB resist, presented in Figure 1c, reveals peaks corresponding to an average mass of 2265.700 Da, indicative of the Zr-based MOC. The observed mass of 2265.700 Da in the MALDI-TOF MS spectrum corresponds to the intact Zr_6 oxo cluster of formula $C_{90}H_{78}O_{35}Zr_6$, comprising six Zr^{4+} ions bridged by oxo and hydroxo ligands, coordinated with 12 benzoate ligands and 4 degradable isopropanol molecules. This composition aligns with the theoretical monoisotopic mass of 2265.866 Da, confirming the expected molecular structure and the +4 oxidation state of zirconium in the cluster.

To further analyze the elemental compositions and chemical bonding of Zr-based MOCs, we employed X-ray photoelectron spectroscopy (XPS). The C 1s spectra (Figure 1d) exhibit four prominent peaks at 284.5, 285.0, 285.6, and 288.4 eV, corresponding to phenyl, C─C, C─O─Zr, and O─C─O, respectively. The O 1s spectrum in Figure 1e displays peaks at 531.3, 529.9, and 531.9 attributed to Zr─O─C, Zr─O─Zr, and Zr─O─H, respectively. Furthermore, the Zr 3d spectra (Figure 1f) exhibit two peaks at 182.2 and 184.5 eV, corresponding to the Zr^{4+} $3d_{5/2}$ and Zr^{4+} $3d_{3/2}$ components, respectively. These are characteristic of Zr^{4+} species, confirming that zirconium exists predominantly in the +4 oxidation state as part of the Zr-oxo cluster.

The particle size distribution of the developed Zr-OCB resist was analyzed using dynamic light scattering (DLS), as shown in Figure S3 (Supporting Information). The average size of the Zr-OCBs is ≈2.7 nm, enabling high-resolution pattern formation. Consequently, the Zr-OCB material demonstrates a carefully engineered structure, making it a promising candidate as a photoresist for next-generation lithography.

We propose that upon electron beam irradiation, cleavage of Zr oxo cluster–benzoate bonds may generate phenyl radicals, initiating a radical crosslinking mechanism.[40,41] When the electron beam irradiates the material, the phenyl group dissociates from the Zr-OCB, leaving carbon radicals that participate in the crosslinking of the backbone, resulting in an insoluble material. This process describes how the Zr-OCB film changes solubility during patterning.

To prove the film composition and chemical changes in the Zr-OCB films during EB exposure, we performed spectroscopic analysis using XPS. **Figures 2b–d** present the core-level C 1s, O 1s, and Zr 3d spectra, respectively, both before and after EB exposure. The experimental data are represented by black dots, with the background and fit shown as red lines. Individual component fits are distinguished by different colored lines specific to each spectrum, as described below.

In the C 1s spectra (Figure 2b), the most intense components (green and blue) at 284.4 and 284.9 eV correspond to phenyl and C─C bonds, attributed to Zr-OCB. Upon EB exposure, the phenyl peaks show a noticeable shift, with a decrease in phenyl peak intensity (from 73.46% to 47.52%) and an increase in C─C peak intensity (from 9.28% to 33.18%). This change is due to the loss of the phenyl group during EB exposure and the subsequent bond formation between carbons containing the carboxylic group at that site.

The O 1s spectra (Figure 2c) show three fitted components at 531.5 eV (Zr─O─C), 532.2 eV (Zr–O–H), and 530.0 eV (Zr─O─Zr), which remain largely unchanged before and after EB exposure. These results suggest that the Zr–oxo cluster is

© 2025 The Author(s). Advanced Materials Technologies published by Wiley-VCH GmbH

2365709x, 0, Downloaded from https://advanced.onlinelibrary.wiley.com/doi/10.1002/admt.202501547 by Ulsan National Institute Of, Wiley Online Library on [13/10/2025]. See the Terms and Conditions (https://onlinelibrary.wiley.com/terms-and-conditions) on Wiley Online Library for rules of use; OA articles are governed by the applicable Creative Commons License

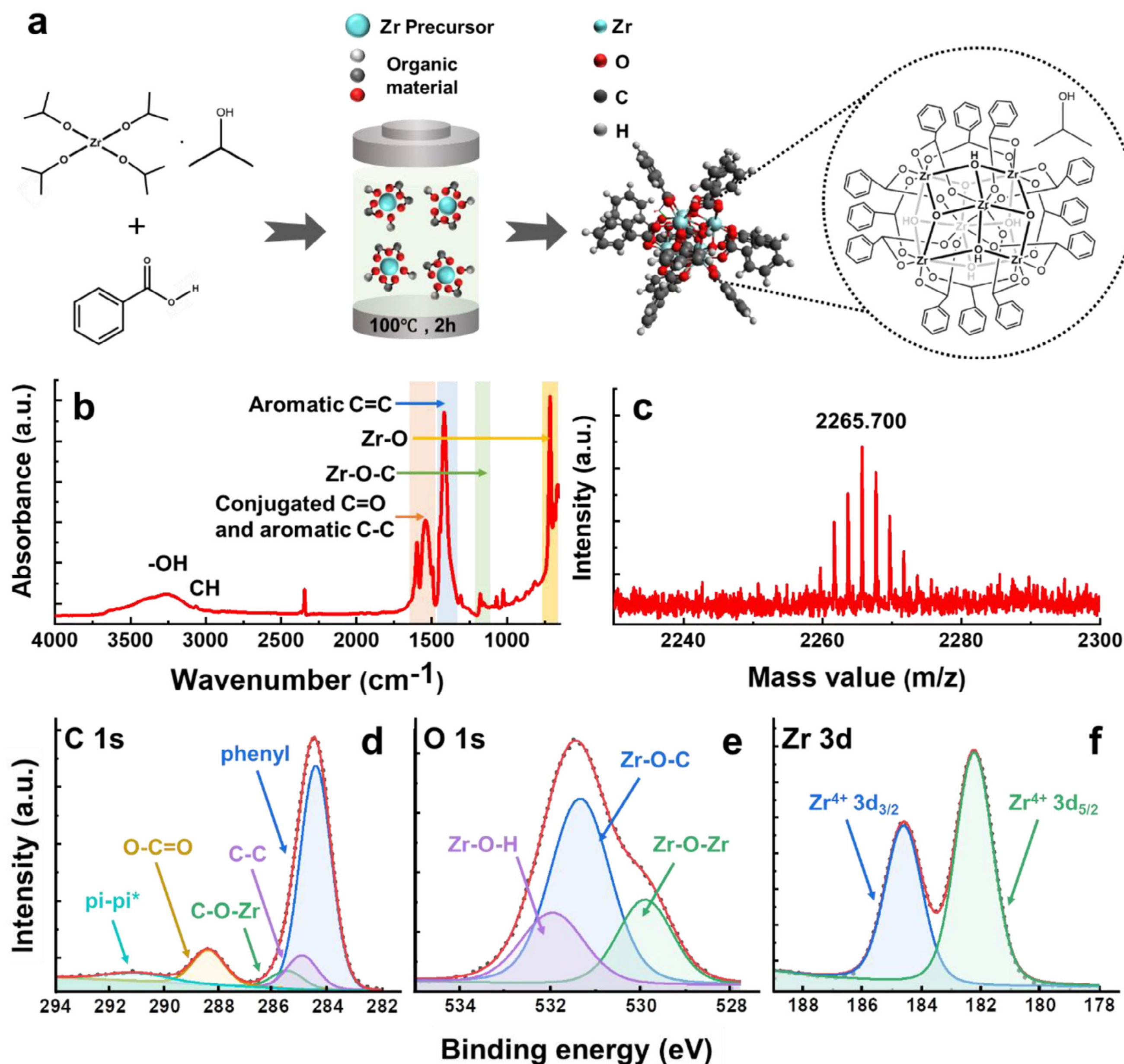

Figure 1. Schematic illustration and structural characteristics of Zr-OCB. a) Schematic of the synthesis process of Zr-OCB. This model is intended to reflect the proposed framework conceptually; b) FT-IR spectra of Zr-OCB; c) MALDI-TOF MS of Zr-OCB; XPS spectra of d) C 1s, e) O 1s, and f) Zr 3d from Zr-OCB.

stable under irradiation, in contrast to the observed changes in the C 1s region. This stability is further supported by quantitative peak area analysis provided in the supporting information (Table S1, Supporting Information).

The Zr 3d spectra (Figure 2d) were analyzed for the spin-orbit-split doublet Zr $3d_{3/2}$ (blue) and Zr $3d_{5/2}$ (green). The Zr 3d spectra, divided into the $3d_{3/2}$ and $3d_{5/2}$ regions for Zr^{4+}, show no change in peak shape or position after EB exposure. This indicates that the phenyl bond is broken upon exposure, increasing the C—C bonds. This increase in C—C bonds reduces solubility in the developer solution, forming a pattern as a negative photoresist.

To further elucidate the detailed patterning mechanism, we analyzed the chemical composition of the surface of Zr-OCB film both before and after EB exposure in Figure 2e. Using a Bi^{+} ion beam (25 keV, 1.2 pA), we calculated the mass of carbonaceous materials in the Time-of-flight secondary ion mass spectrometry (TOF-SIMS) data to understand how the reduction of phenyl groups leads to radical formation and patterning. Characteristic fragment ions such as $C_3H_3^+$, $C_3H_5^+$, $C_3H_7^+$, $C_4H_3^+$, $C_4H_5^+$, $C_4H_9^+$, $C_4H_9O^+$, and $C_6H_5^+$, observed in TOF-SIMS, are derived from the Zr-OCB structure and are consistent with carbon-centered fragments typically formed following radical-induced degradation or crosslinking. The intensity of these ions indicates

 © 2025 The Author(s). Advanced Materials Technologies published by Wiley-VCH GmbH

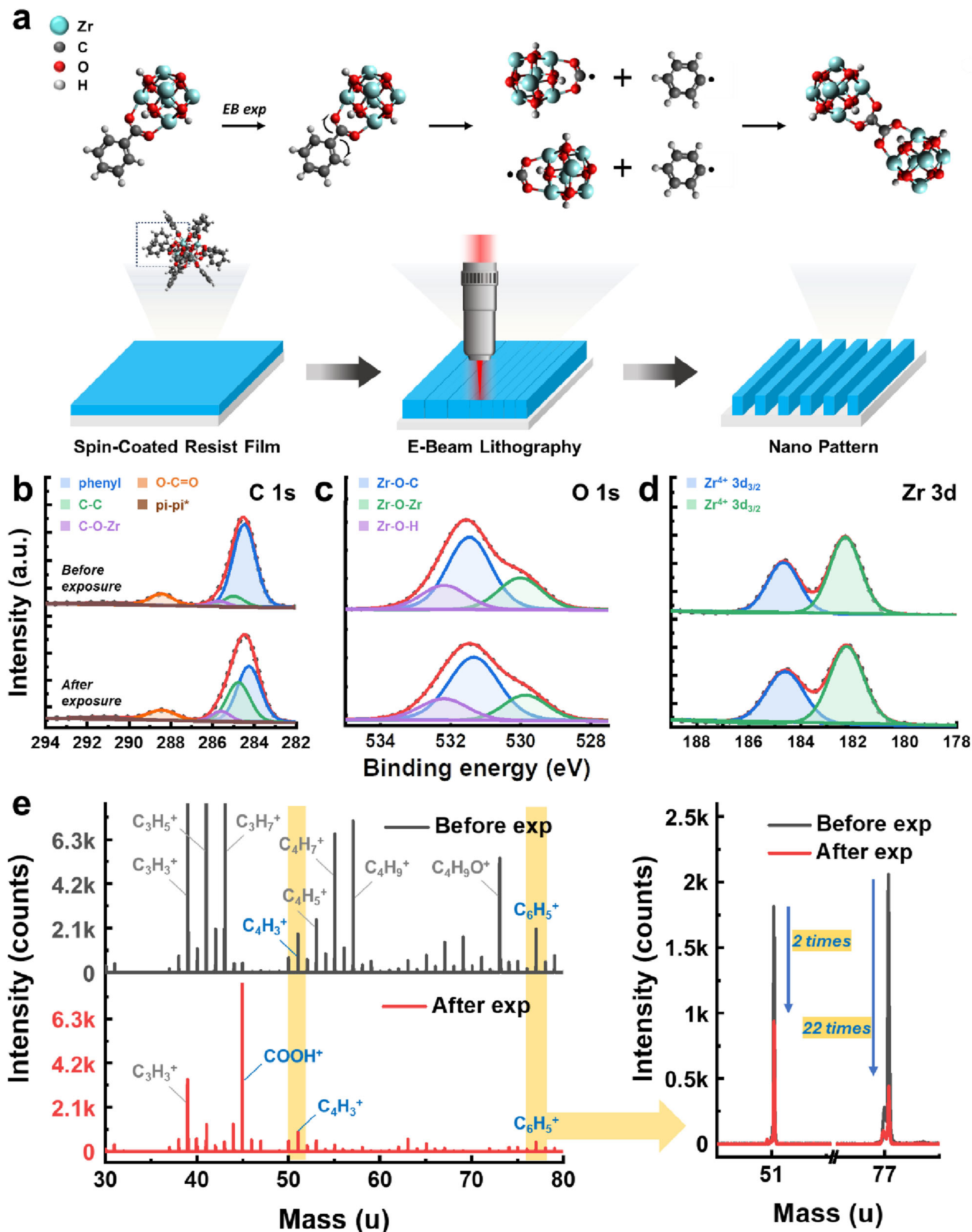

Figure 2. Investigation of the patterning mechanism of Zr-OCB. a) Patterning mechanism for a Zr-OCB resist under EB exposure; XPS spectra obtained before (above graphs) and after EB exposure (below graphs): core-level peaks b) C 1s, c) O 1s, and d) Zr 3d; e) TOF-SIMS positive spectra of Zr-OCB film before and after exposure.

 © 2025 The Author(s). Advanced Materials Technologies published by Wiley-VCH GmbH

2365709x, 0, Downloaded from https://advanced.onlinelibrary.wiley.com/doi/10.1002/admt.202501547 by Ulsan National Institute Of, Wiley Online Library on [13/10/2025]. See the Terms and Conditions (https://onlinelibrary.wiley.com/terms-and-conditions) on Wiley Online Library for rules of use; OA articles are governed by the applicable Creative Commons License

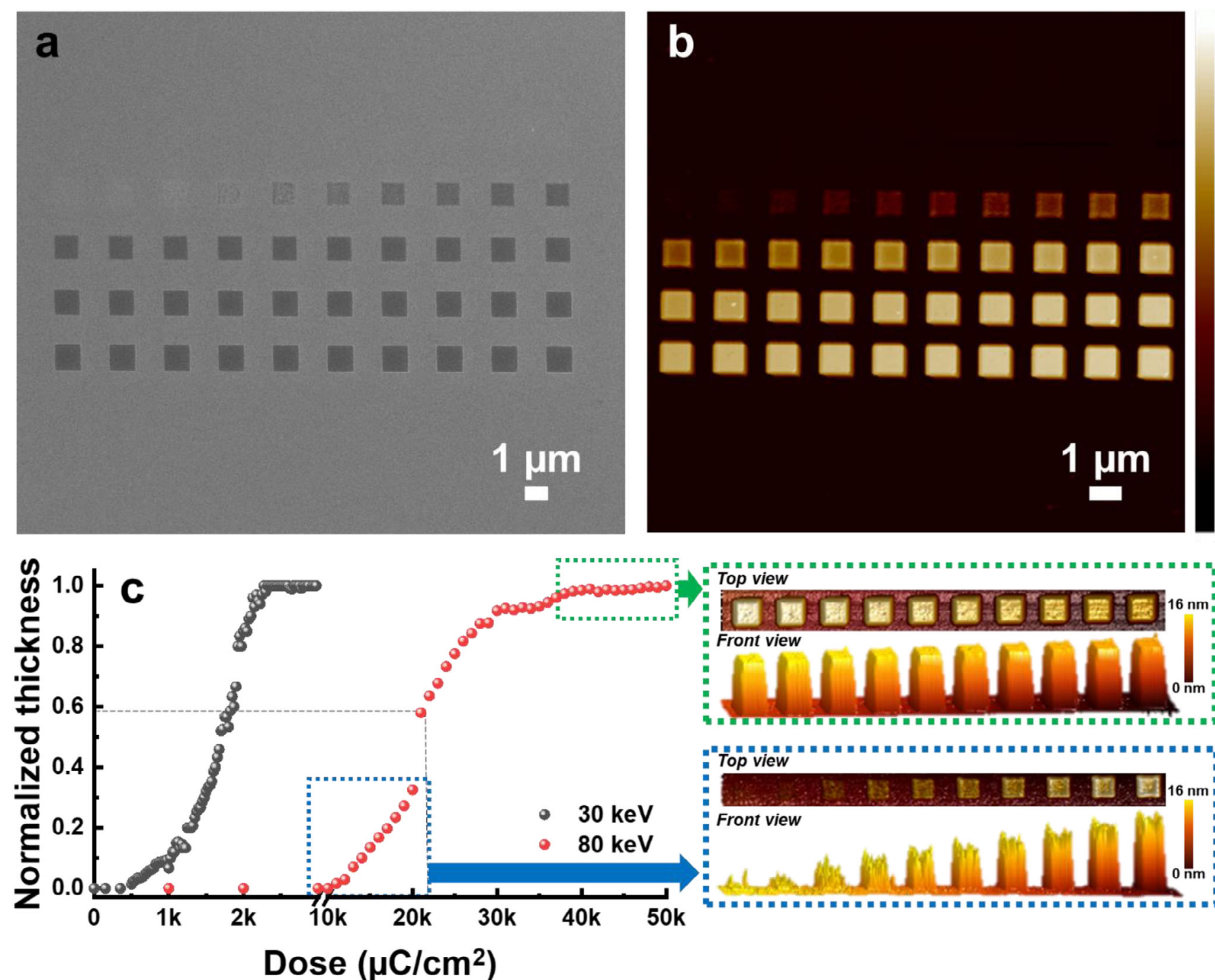

Figure 3. Sensitivity contrast analysis of Zr-OCB for EBL. a) SEM image and b) OM image of 1 × 1 µm patterns exposed using our designed mask with varied doses. c) Sensitivity contrast curves (left) for Zr-OCB resists under 30 and 80 keV EBL, and 3D images (right) showing pattern formation with increasing doses.

the patterning mechanism during exposure. The characteristic ions for the gray colors —$C_3H_3^+$, $C_3H_5^+$, $C_3H_7^+$, $C_4H_5^+$, $C_4H_9^+$, and $C_4H_9O^+$— are derived from tetrahydrofuran, used as a catching solvent. After EB exposure, the Zr-OCB film showed approximately two times lower concentration of $C_4H_3^+$ (m/z 51) and 22 times lower concentration of $C_6H_5^+$ (m/z 77) compared to before exposure. These ions indicate the presence of the phenyl group from benzoic acid, which can engage in the patterning process in EBL. Another significant observation is the increased intensity of $COOH^+$ (m/z 45) when the Zr-OCB film is exposed to the EB source. Although radical-induced decarboxylation of carboxylate ligands is a plausible pathway under high-energy irradiation, TOF-SIMS analysis of the Zr-OCB films after exposure and development reveals clear signals of COOH+ fragments (m/z 45), indicating that a significant portion of the carboxyl groups remains intact. This suggests that complete decarboxylation does not occur under our processing conditions, and residual carboxyl groups likely participate in subsequent condensation or coordination reactions during pattern formation.[42] In summary, TOF-SIMS analysis further supports this proposed pathway: after EB exposure, the $C_6H_5^+$ fragment significantly decreased, while $COOH^+$ signals emerged. These spectral changes are consistent with electron-induced dissociation and suggest the formation of reactive radical intermediates that contribute to the observed crosslinking.

To verify the sensitivity of the Zr-OCB resist to the electron beam source, we exposed the films to a variable dose matrix, as illustrated in Figure S4 (Supporting Information). **Figure 3**a,b show scanning electron microscope (SEM) and optical microscope (OM) images of the exposed patterns using our designed matrix with varying doses. Additionally, we generated a sensitivity contrast curve by exposing the resist film to different doses and measuring the remaining thickness relative to each dose. The sensitivity curve, shown in Figure 3c, was approximated using a generalized logistic function fit. The exposure doses for EBL at 30 and 80 keV ranged from 150 to 3000 and from

© 2025 The Author(s). Advanced Materials Technologies published by Wiley-VCH GmbH

2365709x, 0, Downloaded from https://advanced.onlinelibrary.wiley.com/doi/10.1002/admt.202501547 by Ulsan National Institute Of, Wiley Online Library on [13/10/2025]. See the Terms and Conditions (https://onlinelibrary.wiley.com/terms-and-conditions) on Wiley Online Library for rules of use; OA articles are governed by the applicable Creative Commons License

2365709x, 0, Downloaded from https://advanced.onlinelibrary.wiley.com/doi/10.1002/admt.202501547 by Ulsan National Institute Of, Wiley Online Library on [13/10/2025]. See the Terms and Conditions (https://onlinelibrary.wiley.com/terms-and-conditions) on Wiley Online Library for rules of use; OA articles are governed by the applicable Creative Commons License

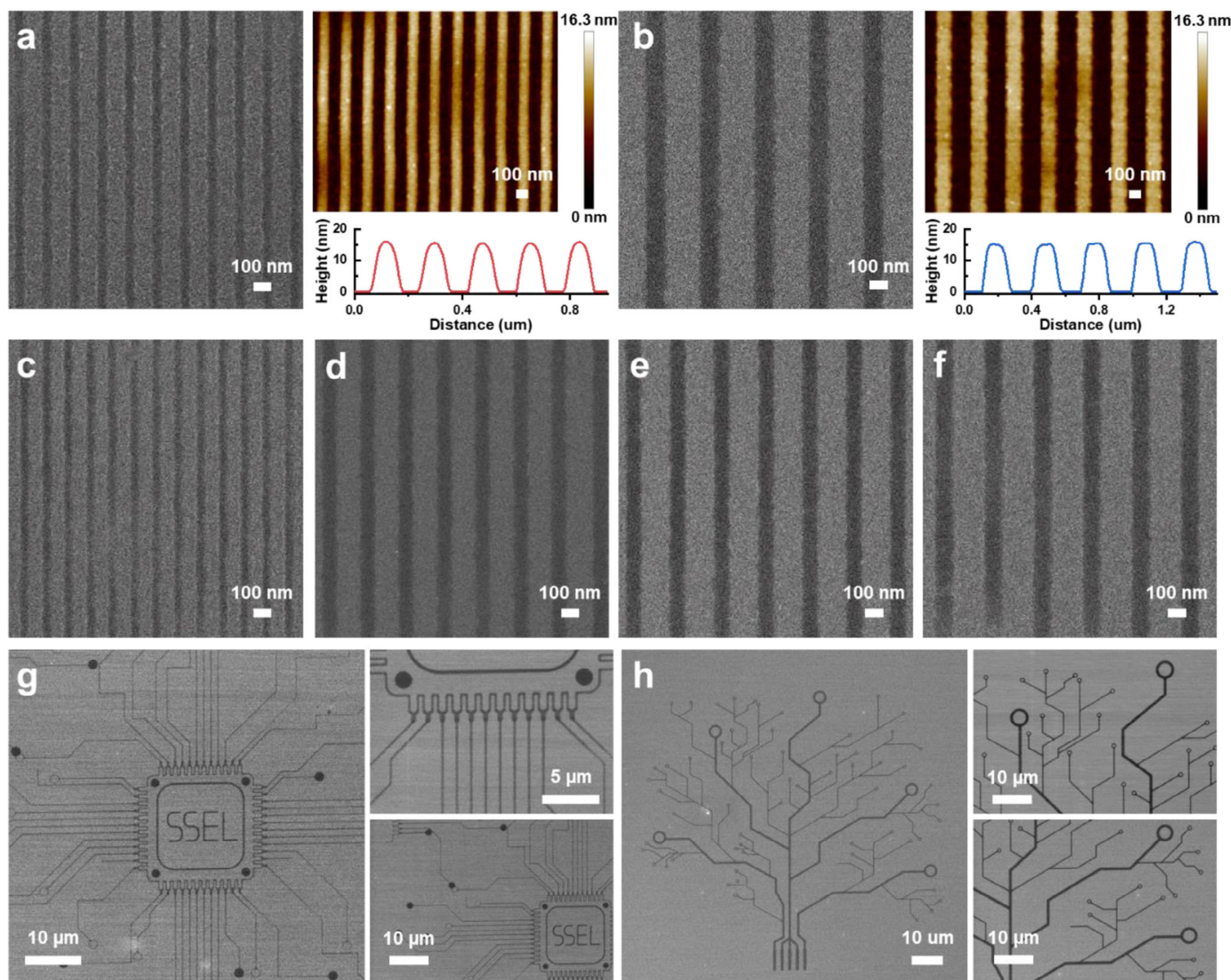

Figure 4. High resolution patterning of 16 nm thick Zr-OCB films for EBL. a,b) SEM (left) and AFM (right) topographic images of the Zr-OCB film with 50 nm line widths a) and 100 nm line widths b) at 2 times the spacing of each line width. c–f) SEM images of the L/2S pattern for the Zr-OCB film with 40 nm (c), 70 nm (d), 80 nm (e), and 90 nm line widths (f). g,h) SEM image of patterned photoresist features.

100 to 50 000 µC cm^{-2}. Thickness values are normalized to the initial film thickness (16 nm) measured prior to exposure. From this curve, we determined the optimal dose for Zr-OCB, which is crucial for photoresist materials. Optimal values were estimated using atomic force microscopy (AFM), with pattern quality assessed through 3D images from OM in the blue and green boxes. Consequently, we achieved a resist sensitivity of 1905 µC cm^{-2} at 30 keV and 20 304 µC cm^{-2} at 80 keV, and a contrast of 1.5 and 1.8, as indicated by the sensitivity curve in Figure 3c. We also assessed the uniformity of the pattern surface after EBL patterning, shown in Figure S5 (Supporting Information). For optimal patterning performance, producing a uniform film is essential. The surface exhibits an RMS roughness of 0.567 nm, nearly identical to the initial roughness of the film (0.428 nm in Figure S6, Supporting Information), indicating high uniformity. Thus, the Zr-OCB resist demonstrates excellent sensitivity and requires less energy for free radical generation to initiate crosslinking.

For effective use as a resist, Zr-OCB must exhibit long-term stability and uniformity in film formation for next-generation EBL applications. We dissolved Zr-OCB in tetrahydrofuran (THF) for use as a resist solution and assessed its stability by exposing it to ambient air at room temperature for 6 months. Zr-OCB is a metal oxo cluster in which benzoic acid is bonded to a zirconium oxo complex. This resistance is stable because the overall charge and the coordination number of the metal are balanced by the combined effect of all the ligands.[43] Evaluation using ^{1}H NMR spectroscopy (see Figure S7, Supporting Information) showed no change in the spectrum, indicating excellent stability of the photoresist.

The Zr-OCB resist was exposed using EBL, and the optimized dose for sensitivity contrast analysis was determined. At the optimized dose, the uniform Zr-OCB thin film produced high-resolution line patterns, as shown in **Figure 4**. The patterns, created in a 16 nm thick Zr-OCB film and developed in tetrahydrofuran, include features of various sizes. Figure 4a,b display 50 nm

© 2025 The Author(s). Advanced Materials Technologies published by Wiley-VCH GmbH

line widths with a 100 nm space and 100 nm line widths with a 200 nm space, respectively, corresponding to the L/2S pattern. Due to the high beam energy used in EBL, patterns smaller than 50 nm (1× the space) were not observed. AFM data (shown in the right panel) confirm that most patterns remain clearly visible, with some minor issues of bridges and residues.

The line patterning for the Zr-OCB resist film achieved an average line width of 50 nm, with variations in spacing between the lines. We also performed L/1S patterning of the Zr-OCB resist, with spacings equal to the line width, as illustrated in Figure S8 (Supporting Information). To evaluate the patterning performance, we analyzed the roughness using SEM images, revealing a line edge roughness (LER) ranging from 1.7 to 4.6 nm, as shown in Figure S9 (Supporting Information). Among these, the line pattern with 2x spacing exhibited an average LER of 3.1 nm. The successful nanopatterning in the EBL tests and the excellent long-term stability of the resist in its solution form highlight its strong potential for practical applications.

In addition, we conducted evaluation tests on various designed pattern features and observed consistent results (Figure 4g,h). All photoresist patterns closely matched the intended designs, showcasing the material's high reactivity and excellent resolution under the exposure source.

Comparing the performance of reported resists is generally challenging due to the varied, non-standardized testing conditions. Despite these limitations, we aim to highlight the advantages of the Zr-OCB resist through a comparison with various EBL materials. We evaluated it in terms of both resist performance and process efficiency, as visualized in Figure S10 (Supporting Information). The comparison is divided into two categories: functional performance and process efficiency. Functional performance includes factors such as resolution, sensitivity, roughness, and structural stability, while process efficiency covers cost-effectiveness, the number of synthesis steps and time, safety, and the absence of additives or extra processes. As shown in Figure S10 (Supporting Information), Zr-OCB particularly excels in process efficiency. It offers a simpler synthesis process and greater cost-effectiveness compared to other materials, and it is also safer, as it avoids the use of strong acids or bases as developers. Additionally, because Zr-OCB does not require extra post-exposure bake (PEB) steps or photoacid generators (PAG), it helps prevent scumming issues that are common with other materials.

3. Conclusion

We demonstrated high-resolution patterning using a carboxylated zirconium-based metal-organic cluster (MOC) resist for electron beam lithography. Incorporation of benzoate ligands into a well-defined Zr oxo cluster enabled efficient crosslinking reactions under electron beam exposure, resulting in uniform, soluble, and spin-coatable thin films. This allowed the formation of sub-40 nm line patterns with a LER of 3.1 nm at an optimized dose. Notably, the Zr-OCB resist operates without the need for PAGs, thereby avoiding common issues such as acid diffusion and thermal instability observed in other metal-based resists. This work demonstrates a distinct direction in metal-based photoresist design by integrating a molecular Zr oxo cluster with benzoate as stable organic ligands and PAG-free crosslinking chemistry. Compared to conventional metal resists, the Zr-OCB platform offers enhanced mechanical integrity, solution stability, and process simplicity, making it a promising candidate for next-generation nanoscale lithography and EUV applications.

4. Experimental Section

Materials: Zirconium (IV) isopropoxide solution (70 wt.% in 1-propanol) (Zr(OCH2CH2CH3)4) (Sigma–Aldrich), Benzoic acid (C_6H_5COOH) (Alfa aesar), *N,N*-Dimethylformamide ($HCON(CH_3)_2$) (SAMCHUN PURE CHEMICAL)

Preparation of Zr-OCB: Zr-OCB was synthesized through a solvothermal reaction utilizing a metal oxo cluster. A solution of zirconium isopropoxide (1.2 mmol, 539 µl) was added to a solution of benzoic acid (1.6 mmol, 147 mg) dissolved in N,N-dimethylformamide (413 mmol, 32 mL). The resulting mixture was dispersed through sonication and then subjected to a 100 °C reaction for 2 h. After the solvothermal process, the product changed from colorless to yellow. The solution was evaporated and precipitated with isopropyl alcohol (IPA). The yellow powder was obtained after drying under vacuum.

Formation of Thin Film for Zr-OCB Resist: Silicon (Si) substrates, each measuring 1 cm by 1 cm, were prepared and cleaned using the RCA process and diluted hydrofluoric acid (HF) to remove the oxidized top layer on the Si surface. The synthesized Zr-OCB resist was dissolved in a tetrahydrofuran solution to create a homogeneous solution through vortex mixing. The concentration of the resist solution was 5 mg mL^{-1}. Before spin-coating, the solution was filtered using a 0.2 µm syringe filter to remove particles of a certain size. The Zr-OCB resist solution was then spin-coated at 3000 rpm for 60 s to create uniform thin films on the Si substrate. The coated film was baked at 90 °C for 60 s in a soft-bake process.

Patterning for E-Beam Lithography: E-beam lithography was performed to demonstrate the feasibility of high-resolution patterning using the Zr-OCB resist. The Zr-OCB films were exposed under a variable dose matrix to analyze the resist's sensitivity. The L/XS patterns were utilized after optimizing the dose for the Zr-OCB resist, where L, X, and S represent line width (L, unit: nm), space width multiplication factor (X), and space width (S, unit: nm), respectively. All patterns were designed using AutoCAD program and produced using a 80 keV electron beam with a 2.1 nm beam size. Subsequently, the films were developed in tetrahydrofuran for 60 s after exposure, and the surface was observed using an SEM. LER was measured using the SEM image for the L/XS pattern through the ImageJ program.

Characterization: Fourier-transform infrared (FT-IR) spectra of the interaction between the Zr oxo cluster and benzoic acid were recorded using a Varian 670 FTIR spectrometer in ATR mode, covering a range of 4000–650 cm^{-1}. Matrix-assisted laser desorption/ionization-time-of-flight mass spectrometry (MALDI-TOF MS) was conducted on a Bruker autoflex max instrument to analyze the molecular weight of Zr-OCB. X-ray photoelectron spectroscopy (XPS) spectra were obtained using a ThermoFisher K-alpha spectrometer with a monochromatic Al Kα irradiation source (1486.6 eV) operating at 600 W. Time-of-flight Secondary Ion Mass Spectrometry (TOF-SIMS) positive spectra were conducted using a TOF–SIMS 5 instrument (ION TOF) with a 10 keV Bi^+ primary ion beam source. Measurements were performed in positive ionization reflector mode (1947 V) with THF as the solvent and DHB as the matrix. The particle size distribution of Zr-OCB was measured by dynamic light scattering (DLS) (Zetasizer Nano-ZS, Malvern Panalytical). Data processing and curve-fitting of the high-resolution spectra were performed using Thermo-advantage software. Scanning electron microscope (SEM) images were captured using a Hitachi High-Technologies S-4800 and a FEI Nanonova 230 instrument equipped with a 15 kV microprobe. Atomic force microscopy (AFM) measurements were conducted using a Bruker Nano Surface Dimension ICON instrument to characterize the surface morphology. E-beam lithography was performed using the NB3 system (Nanobeam Ltd.) with an acceleration voltage of 80 keV and a beam current of 7 nA, and SU5000/ELPHY Multibeam with an acceleration voltage of 30 keV for Schottky FE-SEM with e-beam attachment.

© 2025 The Author(s). Advanced Materials Technologies published by Wiley-VCH GmbH

2365709x, 0, Downloaded from https://advanced.onlinelibrary.wiley.com/doi/10.1002/admt.202501547 by Ulsan National Institute Of, Wiley Online Library on [13/10/2025]. See the Terms and Conditions (https://onlinelibrary.wiley.com/terms-and-conditions) on Wiley Online Library for rules of use; OA articles are governed by the applicable Creative Commons License

Supporting Information

Supporting Information is available from the Wiley Online Library or from the author.

Acknowledgements

This work was supported by the National Research Foundation of Korea (NRF) grant funded by the Korea government (MSIT) (Nos. RS-2020-NR049543 and RS-2025-00553591). This work was partly supported by the 2025 Research Fund (1.250009.01) of UNIST (Ulsan National Institute of Science & Technology and the InnoCORE program of the Ministry of Science and ICT(1.250022). The authors are thankful to the UCRF Center for providing material characterization support.

Conflict of Interest

The authors declare no conflict of interest.

Data Availability Statement

The data that support the findings of this study are available from the corresponding author upon reasonable request.

Keywords

electron beam lithography, metal oxo cluster, organic–inorganic photoresist, patterning

Received: August 4, 2025
Revised: September 7, 2025
Published online:

[1] L. Li, X. Liu, S. Pal, S. Wang, C. K. Ober, E. P. Giannelis, *Chem. Soc. Rev.* **2017**, *46*, 4855.
[2] D. P. Sanders, *Chem. Rev.* **2010**, *110*, 321.
[3] K. Ishikawa, T. Takeda, R. Ogawa, *J. Micro/Nanolithogr. MEMS MOEMS.* **2018**, *17*, 043503.
[4] G. Moody, M. S. Islam, *MRS Bull.* **2022**, *47*, 475.
[5] A. S. Algamili, M. H. M. Khir, J. O. Dennis, A. Y. Ahmed, S. S. Alabsi, S. S. Ba Hashwan, M. M. Junaid, *Nanoscale Res. Lett.* **2021**, *16*, 16.
[6] S. Wang, M. Liu, Y. Feng, Y. Bu, S. H. Huynh, T. W. Ng, F. Gu, A. Yu, X. Jiang, *J. Mater. Chem. A.* **2017**, *5*, 21422.
[7] H. J. Ahn, P. Thiyagarajan, L. Jia, S. I. Kim, J. C. Yoon, E. L. Thomas, J. Jang, *Nanoscale* **2013**, *5*, 1836.
[8] K. Kim, M.-J. Kim, S.-I. Kim, J. Jang, *Sci. Rep.* **2013**, *3*, 3330.
[9] K. Kim, I. Kim, K. Yoon, J. Lee, J. Jang, *J. Mater. Chem. A.* **2015**, *3*, 7706.
[10] H. Xu, V. Kosma, E. P. Giannelis, C. K. Ober, *Poly. J.* **2017**, *50*, 45.
[11] D. Y. Liu, L. Xu, X. Lin, X. Wei, W. J. Yu, Y. Wang, Z. M. Wei, *Chip* **2022**, *1*, 100033.
[12] E. Pascual-San-José, G. Sadoughi, L. Lucera, M. Stella, E. Martínez-Ferrero, G. E. Morse, M. Campoy-Quiles, I. Burgués-Ceballos, *J. Mater. Chem. A.* **2020**, *8*, 9882.
[13] A. H. Gabor, C. K. Ober, *Chem. Mater.* **1996**, *8*, 2282.
[14] V. Jakubek, V. R. Vohra, K. Douki, Y. Kwark, C. K. Ober, *J. Photopolym. Sci. Technol.* **2003**, *16*, 573.
[15] K. Kim, S. Yu, S. W. Kim, T. Kim, S. M. Kim, S. Kang, S. M. Han, J. Jang, *Chem. Commun.* **2017**, *53*, 8172.
[16] H. Sugita, N. Matsumura, *Microelectr. Eng.* **2018**, *195*, 86.
[17] T. Rath, C. Padeste, M. Vockenhuber, C. Fradler, M. Edler, A. Reichmann, I. Letofsky-Papst, F. Hofer, Y. Ekinci, T. Griesser, *J. Mater. Chem. A.* **2013**, *1*, 11135.
[18] J. Liu, H. Guo, M. Li, C. Zhang, Y. Chu, L. Che, Z. Zhang, R. Li, J. Sun, Y. Lu, *J. Mater. Chem. A.* **2021**, *9*, 4262.
[19] R. M. M. Hasan, X. Luo, *Nanomanuf. Metrol.* **2018**, *1*, 67.
[20] M. Yogesh, M. G. Moinuddin, M. Chauhan, S. K. Sharma, S. Ghosh, K. E. Gonsalves, *ACS Appl. Electron. Mater.* **2021**, *3*, 1996.
[21] D. G. H. Shazia Yasin, H. Ahmed, *Microelectron. Eng.* **2002**, *61*, 745.
[22] B. Bilenberg, S. Jacobsen, M. S. Schmidt, L. H. D. Skjolding, P. Shi, P. Bøggild, J. O. Tegenfeldt, A. Kristensen, *Microelectron. Eng.* **2006**, *83*, 1609.
[23] J. R. Wu, T. Lin, Y. Wu, P. Chen, T. S. Gau, B. J. Lin, P. Chiu, R. S. Liu, *Nanoscale Adv.* **2023**, *5*, 3033.
[24] R. Fallica, A. Grenville, A. Frommhold, A. P. G. Robinson, Y. Ekinci, *J. Micro/Nanolith. MEMS MOEMS* **2016**, *15*, 033506.
[25] A. Al-Harbi, M. J. Hammond, G. Parkin, *Inorg. Chem.* **2018**, *57*, 1426.
[26] K. S. Sho Kataoka, *Eur. J. Inorg. Chem.* **2022**, *2022*, 202200050.
[27] Y. Qiao, F. Yan, Z. Liu, X. Wang, J. Xie, G. Shi, J. Wei, J. Zhao, L. Zhang, F. Luo, *Nano Lett.* **2025**, *25*, 7732.
[28] Y. Qiao, O. Zhang, Y. Li, M. Vockenhuber, Y. Ekinci, F. Luo, L. Zhang, *Sci. China Mater.* **2024**, *67*, 3132.
[29] L. V. Parfenova, P. V. Kovyazin, A. K. Bikmeeva, E R. Palatov, *Catalysts* **2020**, *11*, 39.
[30] N. Crespo-Monteiro, A. Valour, V. Vallejo-Otero, M. Traynar, S. Reynaud, E. Gamet, Y. Jourlin, *Materials* **2022**, *15*, 5596.
[31] L. Wu, I. Bespalov, K. Witte, O. Lugier, J. Haitjema, M. Vockenhuber, Y. Ekinci, B. Watts, A. M. Brouwer, S. Castellanos, *J. Mater. Chem. C.* **2020**, *8*, 14757.
[32] S. M. Mohammad, N. T. Saifullah, R. Ganesan, *J. Micro/Nanopattern. Mater. Metrol.* **2022**, *21*, 041402.
[33] J. Jiang, M. Yu, C. K. Ober, *J. Photopolym. Sci. Technol.* **2014**, *27*, 663.
[34] K. Sakai, W. Pan, E. P. Giannelis, C. K. Ober, *J. Photopolym. Sci. Technol.* **2019**, *32*, 711.
[35] S. Yao, L. Z. Dong, Y. L. Li, N. Li, J. Liu, Y. Lan, *Sci. Bull.* **2024**, *69*, 1418.
[36] M. Kumar, R. Bala, V. S. Gondil, S. K. Pandey, S. Chhibber, D. V. S. Jain, R. K. Sharma, N. Wangoo, *J. Mater. Sci.* **2017**, *52*, 8568.
[37] G. Bragaggia, A. Beghetto, F. Bassato, R. Reichenbächer, P. Dolcet, M. Carraro, S. Gross, *Polymers* **2021**, *13*, 3268.
[38] W. Zhao, X. Xiao, G. Pan, Z. Ye, *J. Coat. Technol. Res.* **2019**, *17*, 657.
[39] U. Schubert, *XRD Chem. Rev.* **2022**, *469*, 214686.
[40] L. Junseok, D. B. D, T. Y. John, *J. Am. Chem. Soc.* **2006**, *128*, 6008.
[41] S. Kubosaki, Y. Iwata, Y. Tanaka, K. Osaka, M. Yamawaki, T. Morita, Y. Yoshimi, *J. Org. Chem.* **2020**, *85*, 5362.
[42] F. Cheng, D. W. Grainger, D. G. Castner, *Anal. Chem.* **2007**, *79*, 8781.
[43] U. Schubert, *Coord. Chem. Rev.* **2017**, *350*, 61.

© 2025 The Author(s). Advanced Materials Technologies published by Wiley-VCH GmbH

2365709x, 0, Downloaded from https://advanced.onlinelibrary.wiley.com/doi/10.1002/admt.202501547 by Ulsan National Institute Of, Wiley Online Library on [13/10/2025]. See the Terms and Conditions (https://onlinelibrary.wiley.com/terms-and-conditions) on Wiley Online Library for rules of use; OA articles are governed by the applicable Creative Commons License